# Orbital sensitivity in $Mg^{2+}$ dielectronic recombination calculations

J. Fu,[1] T. W. Gorczyca,[1,*] D. Nikolic,[1] N. R. Badnell,[2] D. W. Savin,[3] and M. F. Gu[4]
[1]*Department of Physics, Western Michigan University, Kalamazoo, Michigan 49008-5252, USA*
[2]*Department of Physics, University of Strathclyde, Glasgow, G4 0NG, United Kingdom*
[3]*Columbia Astrophysics Laboratory, Columbia University, New York, New York 10027, USA*
[4]*Lawrence Livermore National Laboratory, Livermore, California 94550, USA*
(Received 17 November 2007; published 17 March 2008)

We have investigated the reason for significant discrepancies between the results of two recent, similar computational methods [Zatsarinny *et al.*, Astron. Astrophys. **426**, 699 (2004); Gu, Astrophys. J. **590**, 1131 (2003)] for dielectronic recombination (DR) of $Mg^{2+}$. It is found that the choice of orbital description can lead to discrepancies by as much as a factor of 2 between *total* peak DR rate coefficients resulting from otherwise-identical computations. These unexpected differences are attributed to the large sensitivity to bound-orbital relaxation and continuum-orbital description effects on the computed radiative and autoionizing transitions arising from accidental cancellation. In order to obviate these effects, an approach, using a separate, nonorthogonal orbital basis for each configuration, is employed to yield a DR rate coefficient that we assess to be more reliable than all earlier published results.

DOI: 10.1103/PhysRevA.77.032713 PACS number(s): 34.80.Lx, 32.70.Cs, 32.80.Zb

## I. INTRODUCTION

Dielectronic recombination (DR) is the process by which an incident electron collides with an atomic ion to produce an intermediate resonance state that then radiates to a final bound state:

$$e^- + A^{q+} \rightarrow A^{(q-1)+**} \rightarrow A^{(q-1)+*} + h\nu. \quad (1)$$

In astrophysical and fusion-related plasmas, DR is usually the dominant pathway for converting ions of charge $q$ to a lower charge $(q-1)$ and it is also responsible for DR satellite lines [1–5]. It is thus important to have accurate DR rate coefficients available for reliable plasma modeling, which is not always the case.

In response to this need, we have embarked on a program for computing DR data for ions of all isoelectronic sequences of astrophysical and fusion interest [6]. The latest work has treated up through Mg-like sequences using state-of-the-art atomic physics methods [7].

We recently presented calculations for the DR of Ne-like ions forming Na-like ions [8], where our DR rate coefficient results were found to be roughly half the previously recommended data [9]. This we attributed to the various approximations and scalings used in the determination of those earlier recommended rate coefficients [9]. However, we subsequently discovered that our reported DR rate coefficients for the low ionization stages of the Ne-like series—$Mg^{2+}$ in particular—were roughly 50% greater than the results reported in a similar-in-spirit theoretical study [10] (see Fig. 1). Both of these state-of-the-art methods were based on the independent-processes, isolated-resonance, distorted-wave (IPIRDW) approximation. Our multiconfiguration Breit-Pauli (MCBP) approach [11], as used in our earlier study [8], approximates solutions to the Schrödinger equation with first-order relativistic corrections, whereas the flexible atomic code (FAC) [10] instead approximates solutions to the fully relativistic Dirac equation with a similar multiconfigurational representation; but, for such a low nuclear-charged ion such as $Mg^{2+}$, such additional relativistic effects can be safely ruled out as a possible source of discrepancy between these two calculational results. Thus it is surprising that two methods based on the same essential physics should yield such different results. Indeed, several comparisons between MCBP, FAC, and/or the similar multiconfigurational Dirac-Fock (MCDF) methods have noted quite good agreement between results using these three IPIRDW methods for most other ions [8,12–14].

The purpose of the present paper is to explain why two, similar, state-of-the-art theoretical approaches can yield such large differences in computed DR rate coefficients. Furthermore, we present results and assess the reliability of our theoretical approach for such a sensitive case. We have es-

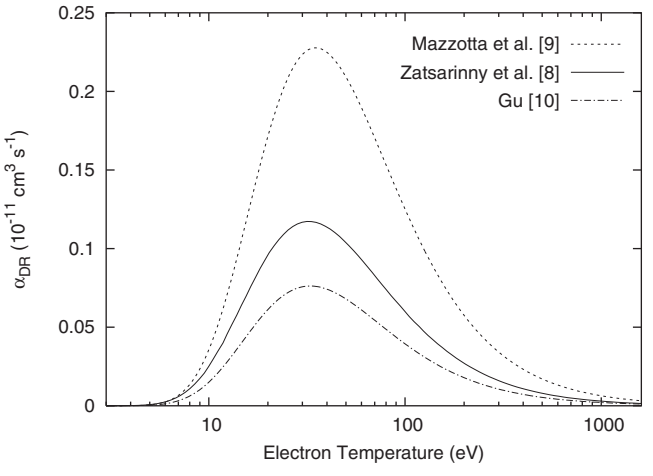


FIG. 1. Comparison of $Mg^{2+}$ DR rate coefficients $\alpha_{DR}(T)$: dashed line, recommended results of Mazzotta *et al.* [9]; solid line, AUTOSTRUCTURE results of Zatsarinny *et al.* [8]; and dash-dot line, flexible atomic code (FAC) results of Gu [10].

*gorczyca@wmich.edu

 

tablished that the original discrepancies were not due to any particular deficiency on the part of either theoretical method; rather, the *choice* of initial atomic bound and continuum orbital description differed between the two published calculations [8,10], and this alone was responsible for the roughly 50% discrepancy between the two.

The rest of the paper is organized as follows. We first give a brief outline of the relevant physical processes in the next section, then we describe our various theoretical atomic physics approaches in Sec. III, including a discussion of the importance of choice of orbitals. Finally, in Sec. IV we compare various theoretical results and also present our recommended [15] results from what we assess to be the most reliable computations—those obtained using a separate nonorthogonal basis description for each initial, intermediate, and final configuration.

## II. THEORETICAL CONSIDERATIONS

The dominant contribution to DR of $Mg^{2+}$ can be described as follows: an initial electron-ion collision state of a free electron incident on a $Mg^{2+}$ ion undergoes dielectronic capture into a doubly excited resonance state, with a rate proportional via detailed balance to the reverse autoionization rate $A_{a1}$, and is then followed by radiative decay to a final bound-state of $Mg^{+}$, with radiative rate $A_r$. This can be described schematically:

$$\begin{array}{c} e^- + \mathrm{Mg}^{2+}(2s^2 2p^6) \\ \updownarrow A_{a1} \\ \overset{A_{ai}}{\mathrm{Mg}^{+}(2s^2 2p^5 3lnl') \rightarrow \mathrm{Mg}^{2+}(2s^2 2p^5 3l'') + e^-} \\ \downarrow A_r \\ \mathrm{Mg}^{+}(2s^2 2p^6 n'l') + h\nu. \end{array} \tag{2}$$

This is inherently a $\Delta n_c > 0$ core excitation with the $2p \rightarrow 3l$ core transitions dominating. The energy averaged DR cross section is proportional to the dielectronic capture rate $A_{a1}$ times the radiate branching ratio for radiative decay, with rate $A_r$, vs autoionization to either the ground or excited continua (with rates $A_{a1}$ and $\Sigma_{i=2}^{n_o} A_{ai}$, respectively):

$$\langle \sigma \rangle \propto A_{a1} \frac{A_r}{A_r + A_{a1} + \sum_{i=2}^{n_o} A_{ai}}. \tag{3}$$

Here, $n_o$ is the number of open channels. This is equal to one up to collision energies of ~49.6 eV (i.e., capture into $n \leq 9$) above which point the $2p^5 3s(^3P) + e^-$ channel opens up. Thus the accuracy of computed DR rate coefficients—Maxwellian averages $\langle v\sigma \rangle$—hinges on the accuracy of the various autoionization and radiative rates.

We find that the dominant contribution to the DR cross section $\sigma$, and therefore to the Maxwellian-averaged DR rate coefficient $\langle v\sigma \rangle$, comes from the $2p^5 3s(^1P)nl$ $(3 \leq n \leq 9)$ resonances (see Fig. 2) that radiate predominantly via $3s \rightarrow 2p$ transitions. This is because for higher-$n$ of this dipole-favored capture resonance series, and indeed for the other strong oscillator strength populated $2p^5 3d(^1P)nl$ series, there are, besides autoionization to the ground level, additional autoionizing channels open that contribute to Eq. (3), and thus there is a sudden drop off of these resonance contributions (see Fig. 3). This is the familiar autoionization-into-excited-states suppression phenomenon [16]. Consequently, the large discrepancies between the otherwise-similar IPIRDW results—the MCBP [8] and FAC [10] DR rate coefficients—can be understood by studying the $2p^5 3s(^1P)nl \rightarrow 2p^6 nl + h\nu$ radiative and $2p^5 3s(^1P)nl \rightarrow 2p^6 + e^-$ autoionization transitions. We begin with a description of our various orbital bases and demonstrate how different choices of orbital optimization affect our computed radiative and autoionization rates that determine the DR rate coefficients.

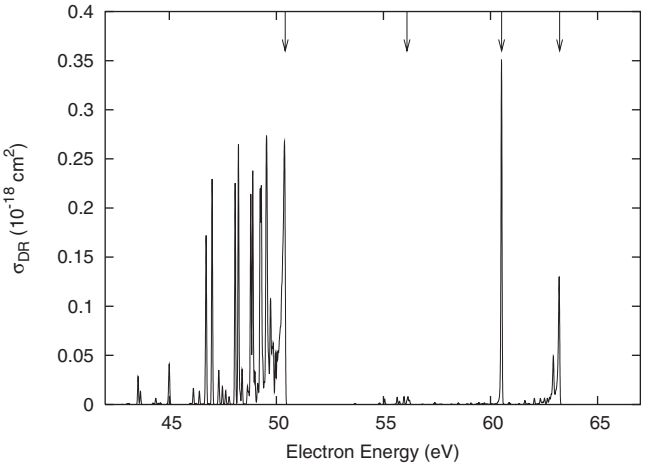


FIG. 2. $Mg^{2+}$ DR cross section $\sigma_{DR}$ convoluted with a full width at half maximum (FWHM) Gaussian of 0.05 eV, indicating that the dominant resonances contributing to the Maxwellian-averaged rate coefficient derives from the $2p^5 3snl$ Rydberg series of resonances. The arrows at the top of the figure show, from left to right, the positions of the $2p^5 3s(^1P_1)$, $2p^5 3p(^1P_1)$, $2p^5 3p(^1S_0)$, and $2p^5 3d(^1P_1)$ thresholds.

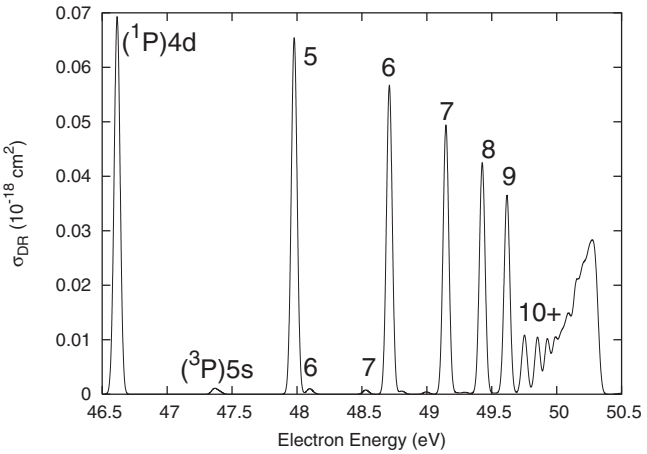


FIG. 3. $2p^6 \epsilon p \rightarrow 2p^5 3s(^1P)nd(^1P^o) \rightarrow 2p^6 nd + h\nu$ contributions to DR of $Mg^{2+}$, showing the dominance of the $n \leq 9$ members. The cross section $\sigma_{DR}$ has been convoluted with a 0.05 eV FWHM Gaussian for clarity.

## III. ORBITAL DESCRIPTIONS

When describing the various atomic wave functions occurring in Eq. (2), it is important to note that the intermediate $Mg^{+}(2s^2 2p^5 3lnl')$ resonance states and the final excited continua $2s^2 2p^5 3l'' + e^-$ differ from the $2s^2 2p^6$ initial ground state of $Mg^{2+}$ in that there are only five $2p$ electrons rather than six. As a result, the $2p$ orbitals in the resonance and/or excited states, which experience a weaker repulsive screening potential due to the screening from only four similar $2p$ electrons, are more compact, or "relaxed," than the more-diffuse $2p$ orbital in the ground state, which is screened by five other $2p$ electrons.

Accounting for relaxation effects can be difficult using conventional atomic structure and collision codes that typically rely on a single, orthogonal set of atomic orbitals in the description of the initial, intermediate, and final states. However, as will be shown below, the so-called *active* $2p$ orbital entering into the calculation of radiative and autoionization rates is in fact the more diffuse "ground" orbital rather than the compact "relaxed" orbital. We have tracked down the underlying cause for the differences between the results of Zatsarinny *et al.* [8] and Gu [10] as being due to the use of orbitals that were optimized on the $Mg^{2+}$ $2s^2 2p^5 3s$ excited state [8] or the $Mg^{+}$ $2s^2 2p^5 3l^2$ intermediate resonance core states [10], respectively.

We describe the effect of using four separate orbital descriptions on the computed radiative and autoionization transitions and, ultimately, on the DR rate coefficient. Utilizing the same atomic structure and collision code AUTOSTRUCTURE [11] as was used in our earlier study [8], these four sets of orbitals are used within otherwise identical DR calculations. The first set of "relaxed" or "$N^*$-electron" orbitals is essentially that used in [8], the second set of "ground" or "$N$-electron" orbitals is our assessment of the "best" orthogonal basis to use, the third set of "resonance" or "$N+1$-electron" orbitals is essentially that used in [10], and the fourth set of nonorthogonal orbitals is what we assess to yield the most reliable DR rate coefficient.

At this point, we should address why a particular choice of orbitals should be so important. After all, provided that adequate configuration-interaction (CI) is included using any complete basis of orbitals, convergence of wave functions should be obtainable. For practical computational purposes, however, only lowest-order CI can be feasibly included, and given especially the strong orbital relaxation effects that exist for our dominant $2 \rightarrow 3$ transitions, the choice of orbital basis can be crucial, as we now demonstrate.

In order to designate the various bases used for the present, otherwise identical, DR calculations, we choose the following. For the case of $Mg^{2+}$, we have an atomic number $A=12$ with a target ion consisting of $N=10$ electrons, with a ground state configuration of $1s^2 2s^2 2p^6$ and the important excited state $1s^2 2s^2 2p^5 3s$ (we shall not consider the closed $1s$ and $2s$ subshells further).

### A. Relaxed ($N^*$) basis

The basis used in our earlier study [8] is designated by the symbol $N^*$ in that the relevant orbitals were determined from a Hartree-Fock (HF) [17] calculation optimized on the $2p^5 3s$ *excited* state. These were then followed by successive frozen-core HF calculations (the $1s$, $2s$, and $2p$ orbitals were not reoptimized) of the $2p^5 3l$ configuration-averaged states for the remaining $\{3p, 3d\}$ orbitals.

### B. Ground ($N$) basis

We also present results using a basis, designated as $N$, for which the $2p$ orbital was determined from a HF calculation optimized on the $2p^6$ ground state, and then the $3l$ orbitals were determined from frozen-core (the $2p$ orbital was not varied) HF calculations for the $2p^5 3l$ excited states.

### C. Resonance ($N+1$) basis

The third basis, which we designate by $N+1$, is essentially that used by Gu [10], as we have confirmed by direct comparison of orbitals. The $2p$ orbital was again determined from a HF calculation for the $2p^6$ state, but the $n=3$ orbitals, that contribute $\approx 15\%$ of the total peak DR rate coefficient via the $2p\epsilon l \rightarrow 3l'3l''$ lower-lying resonances, were optimized instead on three partially weighted HF calculations to describe more accurately these low-lying resonance states. To determine the $3s$ orbital, a HF calculation on the $2p^5 3s^{2.25}$ fictitious state was performed. The $3p$ orbital was then optimized on the $2p^5 3p^{2.5}$ state and the $3d$ orbital was optimized on the $2p^5 3d^2$ state.

### D. Nonorthogonal basis

In the fourth basis, we have implemented a method within the AUTOSTRUCTURE atomic code [11] in which separate orbital basis sets are used to describe each individual configuration and, hence, the initial, intermediate, and final states. The only approximation used in this approach is that the overlap integrals are all assumed to be unity or zero, as if the orbital basis were orthogonal. This is similar to the approach taken by Cowan [22]. Furthermore, the uncertainty introduced by this approximation can be assessed by determining and utilizing the overlap integrals which would otherwise be taken to be unity. The contribution from terms involving overlap integrals taken to be zero can be expected to be of similar magnitude. We have confirmed that this approximation holds quite well for the present case, introducing uncertainties in the computed DR rate coefficient peak of $\approx 5\%$ that are insignificant compared to the discrepancies that we are investigating.

### E. Orbital and rate coefficient comparisons

The relaxed ($N^*$) basis includes somewhat more compact $2p$ orbitals compared to the $N$ and $N+1$ bases, having been optimized with different $2p$ orbital screening. On the other hand, the $3s$ orbital from the $N+1$ basis will be more diffuse than the other two since it was screened by an extra electron in the HF calculation. These orbitals are compared in Fig. 4. At first glance, only slight differences exist overall that would not seem too important. However, the resultant total DR rate coefficient $\alpha_{DR}$, shown in Fig. 5, is seen to differ

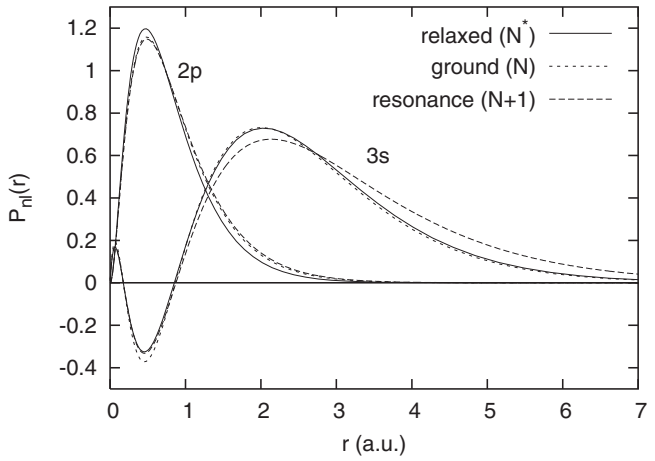


FIG. 4. Comparison of $Mg^{2+}$ orbitals from each orthogonal basis.

appreciably between the three basis sets. In order to understand why seemingly small orbital differences lead to large rate coefficient differences, we examine the computed energies, radiative rates, and autoionization rates that are used in the final DR calculations.

### F. Transition energy differences

Typically, energy uncertainties $\Delta E$ only affect the accuracy of near-threshold $\Delta n_c=0$ rate coefficients due to the corresponding uncertainty in whether a low-lying resonance is above or below threshold [18]. Furthermore, the computed energy position of an above-threshold resonance affects the DR rate coefficient via the $\exp(-E/k_BT)$ Maxwellian distribution term [19] (here $k_B$ is the Boltzmann factor; see also the Appendix). Whether the lower-lying resonances are above or below threshold is not a problem for the present case of Ne-like $Mg^{2+}$ where only $\Delta n_c>0$ processes are possible (the $L$ shell is initially full); even the lowest-lying

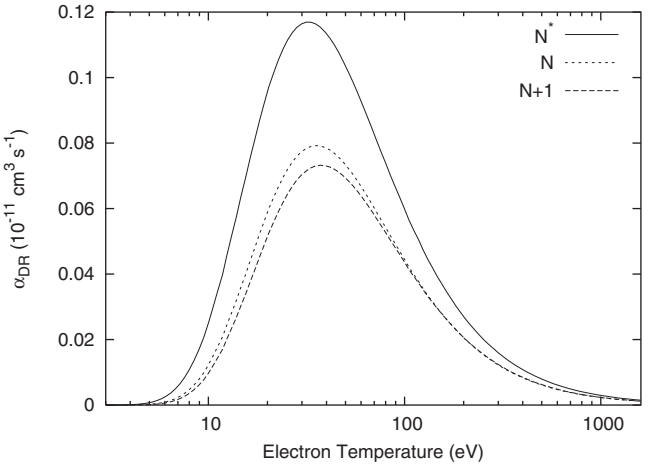


FIG. 5. Comparison of the total DR rate coefficient obtained using each of the three orthogonal bases. The $N^*$ maximum is 60% greater than the $N+1$ maximum.

TABLE I. $Mg^{2+}$ energy levels in Rydbergs.

| Energy level | NIST [20] | $N^*$ | $N$ | $N+1$ | Nonorthogonal |
|---|---|---|---|---|---|
| $2s^22p^6(^1S_0)$ | 0.000 | 0.000 | 0.000 | 0.000 | 0.000 |
| $2s^22p^53s(^3P_2)$ | 3.879 | 3.650 | 3.983 | 4.019 | 3.903 |
| $(^3P_1)$ | 3.890 | 3.661 | 3.995 | 4.030 | 3.914 |
| $(^3P_0)$ | 3.899 | 3.671 | 4.002 | 4.038 | 3.922 |
| $2s^22p^53s(^1P_1)$ | 3.932 | 3.705 | 4.053 | 4.073 | 3.966 |
| $2s^22p^53p(^3S_1)$ | 4.259 | 4.029 | 4.348 | 4.425 | 4.276 |
| $2s^22p^53p(^3D_3)$ | 4.320 | 4.084 | 4.420 | 4.473 | 4.338 |
| $(^3D_2)$ | 4.325 | 4.089 | 4.426 | 4.479 | 4.344 |
| $(^3D_1)$ | 4.333 | 4.097 | 4.433 | 4.486 | 4.351 |
| $2s^22p^53p(^1D_2)$ | 4.351 | 4.113 | 4.460 | 4.501 | 4.374 |
| $2s^22p^53p(^1P_1)$ | 4.359 | 4.123 | 4.467 | 4.508 | 4.380 |
| $2s^22p^53p(^3P_2)$ | 4.364 | 4.127 | 4.471 | 4.512 | 4.385 |
| $(^3P_0)$ | 4.367 | 4.131 | 4.475 | 4.515 | 4.388 |
| $(^3P_1)$ | 4.369 | 4.133 | 4.476 | 4.517 | 4.389 |
| $2s^22p^53p(^1S_0)$ | 4.520 | 4.448 | 4.841 | 4.748 | 4.720 |
| $2s^22p^53d(^3P_0)$ | 4.831 | 4.587 | 4.955 | 4.983 | 4.876 |
| $(^3P_1)$ | 4.834 | 4.590 | 4.957 | 4.985 | 4.878 |
| $(^3P_2)$ | 4.838 | 4.595 | 4.962 | 4.990 | 4.883 |
| $2s^22p^53d(^3F_4)$ | 4.844 | 4.601 | 4.970 | 4.994 | 4.889 |
| $(^3F_3)$ | 4.846 | 4.604 | 4.974 | 4.997 | 4.891 |
| $(^3F_2)$ | 4.855 | 4.612 | 4.981 | 5.003 | 4.898 |
| $2s^22p^53d(^1F_3)$ | 4.857 | 4.615 | 4.986 | 5.006 | 4.901 |
| $2s^22p^53d(^3D_1)$ | 4.868 | 4.627 | 5.001 | 5.016 | 4.911 |
| $(^3D_3)$ | 4.875 | 4.631 | 5.002 | 5.020 | 4.916 |
| $(^3D_2)$ | 4.877 | 4.632 | 5.003 | 5.021 | 4.917 |
| $2s^22p^53d(^1D_2)$ | 4.873 | 4.634 | 5.005 | 5.023 | 4.919 |
| $2s^22p^53d(^1P_1)$ | 4.886 | 4.647 | 5.028 | 5.035 | 4.928 |

$2p^53l'3l''$ resonances are far above the initial $2p^6\epsilon l$ continua. However, we demonstrate in the Appendix that energy differences in computed resonance energies lead to even larger differences in maximum rate coefficients via the $\exp(-E/k_BT)$ Maxwellian distribution term (see also Ref. [19]).

In Table I we compare the target energies computed using all four basis sets. The $N^*$ basis, having been optimized on the excited states, does a poorer job describing the ground state. As a result, the $2p^53l$ states are more converged than the $2p^6$ state and the transition energies are underestimated compared to the NIST values [20]. The $N$ and $N+1$ bases, on the other hand, describe the ground state better than the excited states and as a result overestimate the transition energies. (The nonorthogonal basis yields results close to the NIST values.)

The transition energies in Table I differ by roughly 10%, between the $N^*$ and $N$ or $N+1$ bases, and this leads to a difference of about 15% between respective rate coefficient peaks (see the Appendix). However, the $N^*$ rate coefficient maximum is 60% greater than the $N+1$ maximum (see Fig. 5), so we now look at differences in the radiative and autoionization rates as the source of the remaining ≈45% difference.

### G. Radiative transition differences

Another quantification of the atomic structure description is the radiative transition rates between $Mg^{2+}$ states. Indeed, the DR rate coefficient in Eq. (2) depends on the $3s \rightarrow 2p$ core radiative transition rate. We are ultimately interested in the radiative rate $A_r$, but it is instructive to inspect the individual computed matrix elements that make up the final expression for this rate. For the transition $i \rightarrow f$, where $\psi_i \leftrightarrow 2p^5 3s$ and $\psi_f \leftrightarrow 2p^6$, the two quantities of interest are the transition energy $\omega$ and the line strength $S$. Given our initial and final wave functions, these are computed as the matrix element difference

$$\omega \equiv \langle \psi_i | \mathcal{H} | \psi_i \rangle - \langle \psi_f | \mathcal{H} | \psi_f \rangle \tag{4}$$

and the matrix element

$$S \equiv |\langle \psi_i | \mathcal{D} | \psi_f \rangle|^2, \tag{5}$$

where $\mathcal{H}$ is the $N$-electron Hamiltonian and $\mathcal{D}$ is the (length) $N$-electron dipole operator. It is interesting to note at this point that a first-order error in either wave function ($|\psi\rangle \rightarrow |\psi\rangle + |\delta\psi\rangle$) gives a second-order error in the transition energy ($\langle \delta\psi | \mathcal{H} | \psi \rangle = 0$ variationally) but a first-order error in the line strength ($\langle \delta\psi | \mathcal{D} | \psi' \rangle \neq 0$), so we expect slight inaccuracies in our actual wave functions to be manifested as larger relative uncertainties in line strength than in energy.

Given these two matrix element results, the other quantities of interest are the dimensionless, bounded oscillator strength $gf$ and the radiative rate $A_r$. They are related to the line strength via

$$g_i f_{if} = g_f f_{fi} \equiv gf = \frac{2}{3}\omega S \tag{6}$$

and

$$A_r = \frac{2}{g_i}\omega^2 \alpha^3 gf = \frac{4}{3g_i}\omega^3 \alpha^3 S, \tag{7}$$

on using atomic units, and with $\alpha$ being the fine structure constant. For our specific problem of the transition $2p^5 3s(^1P^o) \rightarrow 2p^6(^1S)$, the initial statistical weight is $g_i = 3$ and the final statistical weight is $g_f = 1$. Thus the radiative rate—that which goes into Eq. (3)—depends on both the transition energy and the line strength, and its final computed value may have fortuitous cancellation of errors associated with each.

A comparison of radiative data is given in Table II. It is seen, first of all, that the $N^*$ radiative rate is greater than the $N$ and $N+1$ bases. In fact, the $N^*/N+1$ ratio is 1.34, or 34% greater, which accounts, once energy difference effects have been considered, for most of the remaining discrepancy between the two rate coefficients.

To study the root of this large line strength difference, given that the orbitals in Fig. 4 do not seem to differ too much, we look at the dependence of line strength on target orbitals. In the independent particle approximation (neglecting higher-order CI effects), we have that the line strength depends on the radial integral via

TABLE II. Radiative data dependence on the choice of orbitals used to describe the $Mg^{2+}$ $2p^5 3s \rightarrow 2p^6$ transition. The transition energy $\omega$ and line strength $S$ are given in atomic units, the weighted oscillator strength $gf = \frac{2}{3}\omega S$ is dimensionless, and the radiative rate $A_r = \frac{2}{3}\omega^2 \alpha^3 gf$ is given in units of $10^9$ $s^{-1}$.

| | NIST [20] | $N^*$ | $N$ | $N+1$ | Nonorthogonal |
|---|---|---|---|---|---|
| $\omega$ | 1.966 | 1.852 | 2.026 | 2.036 | 1.983 |
| $S$ | 0.168 | 0.229 | 0.163 | 0.129 | 0.169 |
| $gf$ | 0.220 | 0.282 | 0.221 | 0.175 | 0.221 |
| $A_r$ | 9.12 | 10.38 | 9.707 | 7.754 | 9.160 |

$$S \propto \left| \int_0^\infty P_{2p}(r) r P_{3s}(r) dr \right|^2, \tag{8}$$

and there must be some reason that this integral is so sensitive to whether the $N^*$ or $N$ orbitals are used. It should be pointed out that, since the $N^*$ basis uses a poor $2p$ orbital for describing the $2p^6$ ground state, there is significant correlation from the $2p^5 3p$ configuration and this also contributes to the line strength computation.

In Fig. 6, we show the radial integrand for all three cases. It is seen that there is a significant cancellation between the positive and negative contributions to the radial integral determining the line strength and subsequently the radiative rate and the DR strength. This makes the integral more sensitive to slight variations. Thus the larger-$r$ contribution is more important, and here we see that the relaxed $N^*$ $2p$ orbital has a smaller amplitude and contributes less; but, the correction due to the $2p^5 3p$ mixing for the $N^*$ relaxed case, which is zero by Brillouin's theorem [21,22] for the $N$ and $N+1$ cases, turns out in this case to overcompensate and as a result, the $N^*$ computed line strength is too large compared to the NIST [20] value. Thus we would expect that the $N^*$ rate coefficient, like that in our earlier study [8], is an overestimate of the true value, and the $N+1$ result, like that in [10], is an underestimate. Before quantifying this further,

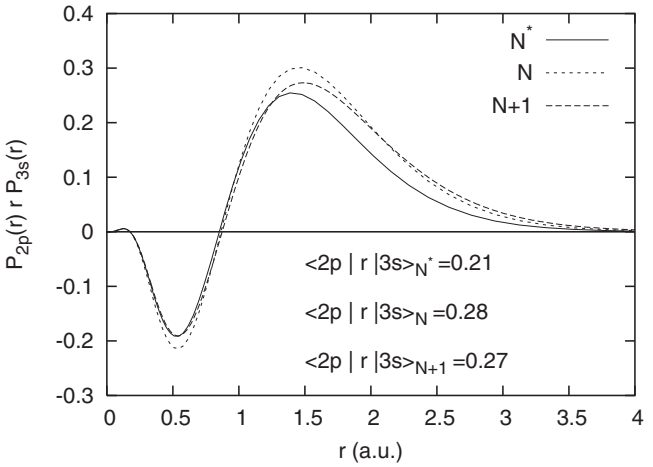


FIG. 6. Comparison of the $Mg^{2+}$ radial integrands $rP_{2p}(r)P_{3s}(r)$.

however, we look at the autoionization transitions in the next section.

The near-cancellation of positive and negative integrands toward the total (but still dominant) $3s \rightarrow 2p$ radiative transition resembles that of the phenomenon in photoionization—the reverse process of DR in most ways—commonly referred to as a *Cooper minimum* [23]. In that case, a continuum orbital $\epsilon l \pm 1$, with energy-dependent nodal variation, inevitably reaches a low-energy point at which the radial integral with the bound electron $nl$, which has absorbed the incident photon, goes through zero, i.e., $\langle \epsilon l \pm 1 | r | nl \rangle = 0$ [24,25].

### H. Autoionization transition differences

In addition to the radiative rate $A_r$, the final determination of our DR rate coefficient from Eq. (3) also depends on the various autoionization rates. For the important initial capture and autoionization $2p^5 3snl \rightarrow 2p^6 + e^-$, we have

$$A_{a1} \equiv 2\pi |\langle \Psi_i | \mathcal{V} | \Psi_f \rangle|^2, \tag{9}$$

with $\Psi_i \leftrightarrow 2p^5 3snl$, $\Psi_f \leftrightarrow 2p^6 \epsilon l \pm 1$, and $\mathcal{V}$ is the electron-electron interaction operator. In the independent particle approximation, this rate depends on the two-dimensional integral

$$A_{a1} \propto \left| \int_0^\infty P_{nl}(r) P_{\epsilon l \pm 1}(r) dr \left( \frac{1}{r^2} \int_0^r P_{2p}(r') r' P_{3s}(r') dr' + r \int_r^\infty P_{2p}(r') \frac{1}{r'^2} P_{3s}(r') dr' \right) \right|^2. \tag{10}$$

We see again that the autoionization rate is dependent on the overlap of the $2p$ and $3s$ orbitals, and so we expect the same sensitivity to orbital description as we found for the radiative rate. Additionally, however, there is an explicit dependence on the (distorted wave) valence electron $nl$ and the resultant continuum orbital $\epsilon(l \pm 1)$. In our earlier study [8], these orbitals were generated using a Thomas-Fermi-Dirac-Amaldi (TFDA) model potential [26]; the valence and continuum orbitals have usually been found to be insensitive to this choice. However, given the extra sensitivity to orbitals in this DR process, it seemed natural to investigate the dependence of valence and continuum orbital descriptions. In addition to the TFDA model potentials, AUTOSTRUCTURE [11] also has the capability of utilizing Slater-type-orbital (STO) model potentials [27] to generate the orbital basis. Both model potentials contain adjustable radial scaling parameters, one per radial orbital, which can be optimized by minimizing a weighted-sum of eigenenergies, say. The resultant STO values are much closer to unity than the TFDA. This is important for consideration of Rydberg and continuum orbitals, for which no direct optimization is possible and a default value of unity is normally assumed. It turns out that for this case, the $N$ and $N+1$ DR rate coefficients were independent of which method (TFDA or STO) was used, as is usually the case, as we have found. However, there was unexpected sensitivity to which model was used for the $N^*$ case. In Fig. 7, we compare the total DR rate coefficient for the $N^*$ case using both models. We see that by using the more accurate (see below) STO model potential method, a much larger rate coefficient is obtained.

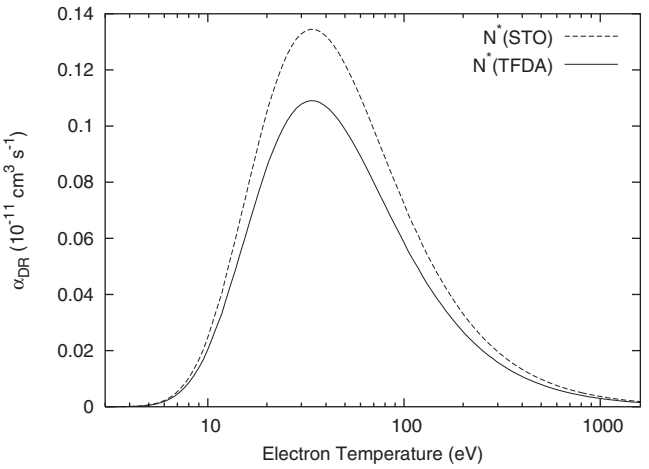


FIG. 7. Comparison of $Mg^{2+}$ DR rate coefficients obtained using STO and TFDA model potentials for the valence and continuum orbitals, and the relaxed $N^*$ bound orbitals.

An assessment of which valence and continuum orbitals to use for the final $N^*$ case can be determined by studying these orbitals and comparing them to the most reliable HF results for a given case. Unlike the TFDA and STO approaches, the HF method uses no approximations and instead solves the complete self-consistent field equations including the nonlocal exchange potential (the TFDA and STO methods approximate this with a local potential). We choose the specific process $2p^6 \epsilon d(^2D^e) \leftrightarrow 2p^5 3s(^1P^o) 5p(^2D^e)$ since we narrowed down this particular transition as leading to the greatest difference between the two methods (see Fig. 8). We

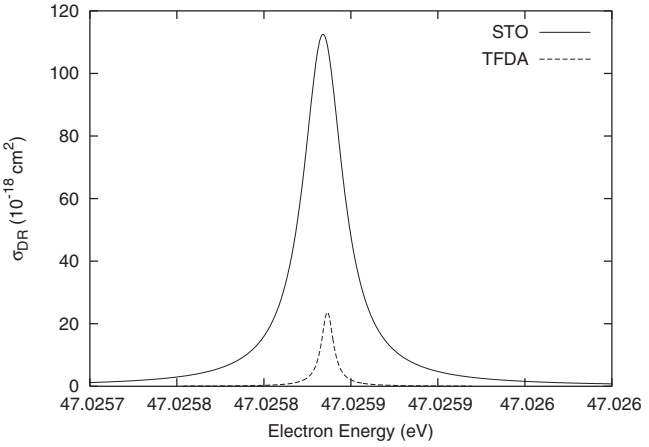


FIG. 8. Partial DR cross section contribution $\sigma_{DR}$ from the (LS) $2p^6 \epsilon d(^2D^e) \rightarrow 2p^5 3s(^1P^o) 5p(^2D^e) \rightarrow 2p^6 5p(^1P^o) + h\nu$ process. The relaxed ($N^*$) basis was used for the $2p$ and $3s$ bound orbitals whereas the valence and continuum orbitals were determined from an optimization on the $2p^5 3s5p$ and $2p^6 \epsilon d$ states, for the $5p$ and $\epsilon d$ orbitals, respectively, using either the STO (solid line) or TFDA (dashed line) methods.

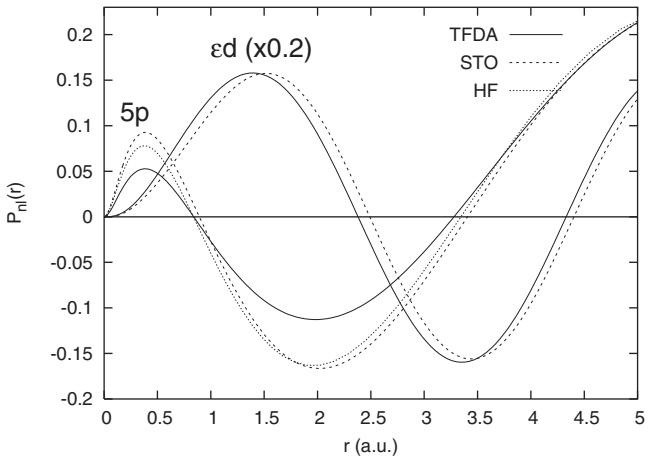


FIG. 9. Comparison of two different "relaxed" (or $N^*$-electron) $5p$ and $\epsilon d$ orbitals generated by AUTOSTRUCTURE using STO (dotted line) and TFDA (solid line) model potentials.

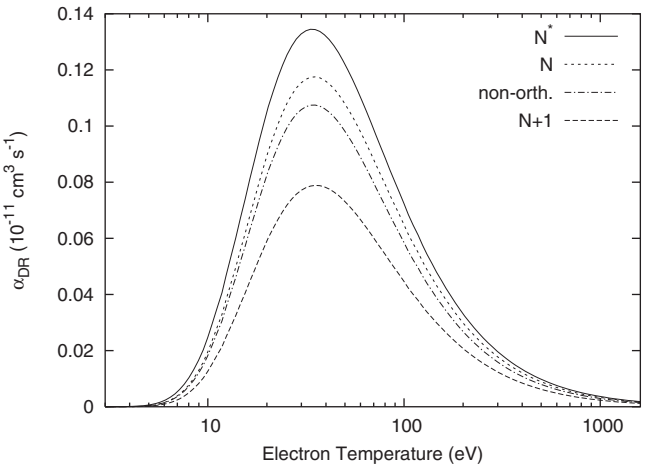


FIG. 10. Final $\alpha_{DR}$ comparison using shifted energies and STO potential DW orbitals. We assess the final nonorthogonal basis result to be the most reliable, and ironically, this is in fairly close agreement with our originally published result (see Zatsarinny *et al.* [8], also shown in Fig. 1, and the $N^*$ results in Fig. 5).

restrict ourselves to a nonrelativistic *LS*-coupling calculation for the clearest demonstration. It is seen that the TFDA results for this particular transition show a very weak DR resonance compared to the STO result. This is because the TFDA autoionization rate $A_{a1}$, coincidentally, has a much smaller value. We have tracked it down to a near cancellation in the two-dimensional integral in Eq. (10), similar to the Cooper minimum phenomena discussed above.

In Fig. 9, the orbitals of interest are shown. At present, it is only possible for us to generate bound HF orbitals. It is seen that the STO potential and HF $5p$ orbitals are in good agreement, but the TFDA potential $5p$ orbital differs considerably. It is this difference that leads to the near cancellation in the integral of Eq. (10). Given that the STO potential orbitals agree best with the most accurate HF orbitals, we assess that the use of STO potential orbitals is a more reliable approach and we shall use these for final comparison.

## IV. FINAL RESULTS

For our final results, we use STO potential distorted waves. Furthermore, to filter out any energy difference effects, we adjust all theoretical thresholds to the NIST values. The DR rate coefficient obtained from all four basis sets is shown in Fig. 10. Given the good agreement in energies and radiative rates between the nonorthogonal basis and the NIST [20] values, we assess the nonorthogonal rate coefficient to be the most reliable, and these values are listed in our recommended database [15]. Ironically, the final nonorthogonal result shown in Fig. 10 is very close to the original relaxed-orbital case (Zatsarinny *et al.* [8] in Fig. 1 and $N^*$ in Fig. 5) using TFDA potential distorted wave orbitals. However, we now know that those earlier results (1) underestimated the transition energy since the excited states were described more accurately than the ground state, (2) overestimated the line strength due to the poor choice of the $2p$ orbital, and (3) underestimated certain autoionization rates due to a poorer choice of TFDA potential distorted wave orbitals rather than the more reliable STO distorted wave potential orbitals, and these three effects fortuitously largely canceled each other in such a way that the final reported DR rate coefficient lines up with the more accurate nonorthogonal basis result. The latter does not suffer from any of those three difficulties.

## V. CONCLUSION

We have investigated the cause of the ≈50% difference in computed $Mg^{2+}$ DR rate coefficients between our earlier MCBP calculations [8] and the earlier FAC calculations [10]. The primary reason for this discrepancy was the use of inappropriate bound orbitals in each case. For the MCBP calculations, a poor $2p$ orbital was used, since it was determined from a Hartree-Fock excited-state optimization, and this resulted in a radiative rate that was greater than the NIST value. The FAC calculations, on the other hand, used a good $2p$ orbital but a poor $3s$ orbital; the latter was determined from more of a resonance-state $2p^5 3s^2$ optimization rather than on the more accurate $2p^5 3s$ excited state, and resulted in a smaller radiative rate. Other factors were the use of incorrect energies—they were smaller than NIST for the MCBP calculations and greater than NIST for the FAC calculations—and an accidental near cancellation in the autoionization matrix element when using the less-reliable TFDA potential for generating distorted waves.

By using a nonorthogonal basis, where the orbitals for the initial, intermediate, and final configurations can all be optimized separately, no inappropriate orbitals are used and we assess these final results to be the most accurate. The entire Ne-like isoelectronic sequence has been recomputed and the new data are available in our database [15], although only the lower ionization stages of the sequence were affected significantly by these orbital sensitivity effects.

As a final note, it needs to be emphasized that the present orbital sensitivity is so pronounced because we are dealing with Ne-like $Mg^{2+}$ for which the entire $n=2$ $L$ shell is occu-

pied. Therefore the only DR resonances that occur are derived from $\Delta n>0$ $(2\rightarrow 3)$ core excitations, giving rise to strong relaxation effects. For ions with a partially filled shell, $\Delta n=0$ core excitations can often dominate the DR process. For these excitations, relaxation effects are less pronounced, and thus we expect that for open shell systems, there will generally (though not always) be less orbital sensitivity and results from calculations using orbitals optimized on the initial, intermediate, or final states will be in better accord.

## ACKNOWLEDGMENTS

J.F. and T.W.G. were supported in part by NASA Astronomy and Physics Research and Analysis (APRA) Program Grant No. NNG0-4GB58G. D.N. and T.W.G. were also supported in part by NASA SHP SR&T Grant No. NNG05GD41G. N.R.B. was supported in part by UK PPARC Grant No. PPA/G/S2003/00055. D.W.S. was supported in part by NASA APRA Grant No. NNG06WC11G and NASA SHP SR&T Grant No. NNG06GD286G. M.F.G. was supported in part by NASA Grants No. NAG5-5419 and No. NNGG04GL76G.

## APPENDIX: EFFECT OF RESONANCE ENERGY DIFFERENCES ON COMPUTED DR RATE COEFFICIENTS

The DR rate coefficient $\alpha_{DR}(T)$ as a function of temperature $T$ is given as a Maxwellian average $\langle v\sigma(E)\rangle$ of the velocity times the DR cross section:

$$\alpha_{DR}(T)=\int_0^\infty 2\pi^{1/2}(k_BT)^{-3/2}Ee^{-E/k_BT}\sigma_{DR}(E)dE. \quad \text{(A1)}$$

Here we assume that we have two resonances of equal strength but different energy positions $E_1$ and $E_2$:

$$\sigma_i(E)=\frac{A}{E}\delta(E-E_i), \quad \text{(A2)}$$

where $A$ is the same for both resonances and the factor of $1/E$ gives the correct energy normalization [28].

The contribution to the rate coefficient from each resonance is therefore

$$\alpha_{DR}^i(T)=\pi^{1/2}Ae^{-E_i/k_BT}(k_BT)^{-3/2}, \quad \text{(A3)}$$

which peaks at $k_BT=\frac{2E_i}{3}$ with a value of

$$\max[\alpha_{DR}^i(T)]=\pi^{1/2}Ae^{-3/2}\left(\frac{2E_i}{3}\right)^{-3/2}, \quad \text{(A4)}$$

giving a ratio between the maxima of the two contributions

$$R_{12}=\frac{\max[\alpha_{DR}^1(T)]}{\max[\alpha_{DR}^2(T)]}=\left(\frac{E_2}{E_1}\right)^{3/2}. \quad \text{(A5)}$$

For a given energy difference $\Delta E_{12}=E_2-E_1$, this introduces a relative ratio difference given by

$$\frac{\Delta R_{12}}{R_{12}}=\frac{3}{2}\frac{\Delta E_{12}}{E_1}, \quad \text{(A6)}$$

so a relative energy difference of, say, 10% leads to a relative ratio difference of 15%.

[1] J. Dubau and S. Volonte, Rep. Prog. Phys. **43**, 199 (1980).
[2] B. Ali, R. D. Blum, T. E. Bumgardner, S. R. Cranmer, G. J. Ferland, R. I. Haefner, and G. P. Tiede, Publ. Astron. Soc. Pac. **103**, 1182 (1991).
[3] P. Beiersdorfer, G. V. Brown, M.-F. Gu, C. L. Harris, S. M. Kahn, S.-H. Kim, P. A. Neill, D. W. Savin, A. J. Smith, S. B. Utter, and K. L. Wong, *Proceedings of the International Seminar on Atomic Processes in Plasmas, NIFS Proceedings Series No. NIFS-PROC-44* (National Institute for Fusion Studies, Nagoya, Japan, 2000), edited by T. Kato and I. Murakami, pp. 25–28.
[4] K. J. H. Phillips, J. Dubau, J. Sylwester, and B. Sylwester, Astrophys. J. **638**, 1154 (2006).
[5] D. W. Savin, Rev. Mex. Astron. Astrofis. **9**, 115 (2000).
[6] N. R. Badnell, M. G. O'Mullane, H. P. Summers, Z. Altun, M. A. Bautista, J. Colgan, T. W. Gorczyca, D. M. Mitnik, M. S. Pindzola, and O. Zatsarinny, Astron. Astrophys. **406**, 1151 (2003).
[7] Z. Altun, A. Yumak, I. Yavuz, N. R. Badnell, S. D. Loch, and M. S. Pindzola, Astron. Astrophys. **474**, 1051 (2007).
[8] O. Zatsarinny, T. W. Gorczyca, K. Korista, N. R. Badnell, and D. W. Savin, Astron. Astrophys. **426**, 699 (2004).
[9] P. Mazzotta, G. Mazzitelli, S. Colafrancesco, and N. Vittorio, Astron. Astrophys. Suppl. Ser. **133**, 403 (1998).
[10] M. F. Gu, Astrophys. J. **590**, 1131 (2003).
[11] N. R. Badnell, J. Phys. B **19**, 3827 (1986); **30**, 1 (1997).
[12] D. W. Savin, S. M. Kahn, G. Gwinner, M. Grieser, R. Repnow, G. Saathoff, D. Schwalm, A. Wolf, A. Müller, S. Schippers, P. A. Zavodszky, M. H. Chen, T. W. Gorczyca, O. Zatsarinny, and M. F. Gu, Astrophys. J. **147**, 421 (2003).
[13] D. W. Savin, G. Gwinner, M. Grieser, R. Repnow, M. Schnell, D. Schwalm, A. Wolf, S.-G. Zhou, S. Kieslich, A. Müller, S. Schippers, J. Colgan, S. D. Loch, N. R. Badnell, M. H. Chen, and M. F. Gu, Astrophys. J. **642**, 1275 (2006).
[14] O. Zatsarinny, T. W. Gorczyca, J. Fu, K. T. Korista, N. R. Badnell, and D. W. Savin, Astron. Astrophys. **447**, 379 (2006).
[15] http://amdpp.phys.strath.ac.uk/tamoc/DATA/DR/.
[16] V. L. Jacobs, J. Davis, P. C. Kepple, and M. Blaha, Astrophys. J. **211**, 605 (1977).
[17] http://www.vuse.vanderbilt.edu/~cff/mchf_collection/
[18] H. Nussbaumer and P. J. Storey, Astron. Astrophys. **126**, 75 (1983).
[19] S. Schippers, M. Schnell, C. Brandau, S. Kieslich, A. Müller, and A. Wolf, Astron. Astrophys. **421**, 1185 (2004).
[20] http://physics.nist.gov/cgibin/AtData/main_asd.
[21] L. Brillouin, J. Phys. Radium **3**, 373 (1932).
[22] R. D. Cowan, *The Theory of Atomic Structure and Spectra* (University of California Press, Berkeley, 1981).

[23] J. W. Cooper, Phys. Rev. **128**, 681 (1962).
[24] D. R. Bates, Mon. Not. R. Astron. Soc. **106**, 432 (1946).
[25] M. J. Seaton, Proc. R. Soc. London, Ser. A **208**, 418 (1951).
[26] W. Eissner and H. Nussbaumer, J. Phys. B **2**, 1028 (1969).
[27] A. Burgess, H. E. Mason, and J. A. Tully, Astron. Astrophys. **217**, 319 (1989).
[28] See, for example, E. Merzbacher, *Quantum Mechanics*, 3rd ed. (Wiley, New York, 1998).